Progress In Electromagnetics Research C, Vol. 172, 174–182, 2026

PIER C

(Received 17 May 2026, Accepted 29 June 2026, Scheduled 4 August 2026)

A Compact CPW-Fed Slotted Patch Antenna with Defective Ground for Wideband RF Energy Harvesting

Vijetha[1,*], K. M. Sudharshan[1], and Sandeep Kumar[2]

[1]*School of Electronics and Communication Engineering, Reva University, Bengaluru 560064, India*
[2]*Special Centre for Nanosciences, JNU, New Delhi, India*

ABSTRACT: A compact wideband antenna suitable for RF energy harvesting applications is presented in this paper. The proposed antenna consists of a slotted rectangular radiating patch excited by a coplanar waveguide (CPW) feed and implemented on an FR4 substrate with overall dimensions of $40 \times 40 \times 1.6\,\text{mm}^3$. A wide impedance bandwidth is achieved through the combined use of a hybrid hexagonal defective ground structure (DGS) and multi-slot loading of the radiating patch, where the patch is embedded within the slotted ground plane to achieve size reduction and enhanced impedance matching. The antenna exhibits a measured impedance bandwidth of 3.61 GHz ($|S_{11}| \leq -10\,\text{dB}$) ranging from 2.18 GHz to 5.79 GHz, covering the Wi-Fi and sub-6 GHz 5G frequency bands. Stable radiation characteristics are observed across the operating band, with a figure-of-eight radiation pattern, a peak gain of 3.67 dB at 3 GHz, and a minimum gain of 2.73 dB at 5 GHz. The antenna exhibits radiation efficiency greater than 95% throughout the operating band, with a maximum value approaching 98%. The antenna is designed and optimized using ANSYS HFSS and experimentally validated through Vector Network Analyzer and anechoic chamber measurements, showing good agreement between simulated and measured results. Owing to its wide bandwidth, compact size, and stable radiation performance, the proposed antenna is well-suited for wideband RF energy harvesting, with future integration into a rectenna system.

1. INTRODUCTION

The increasing proliferation of wireless communication systems operating across multiple frequency bands has resulted in a dense ambient electromagnetic environment. Frequency bands such as Wi-Fi (2.4/5 GHz) and sub-6 GHz 5G are continuously occupied, making them attractive sources for ambient RF energy harvesting to power low-energy electronic devices, wireless sensor nodes, and Internet of Things (IoT) applications. In such systems, the antenna plays a critical role, as it must simultaneously offer wide impedance bandwidth, compact size, stable radiation characteristics, and high radiation efficiency.

Conventional narrowband antennas are inadequate for radio-frequency (RF) energy harvesting, as they can capture energy only from limited frequency ranges. Consequently, wideband and multiband antennas have attracted significant research interest. Among various feeding techniques, coplanar waveguide (CPW) feeding has emerged as a preferred choice due to its low radiation loss, ease of fabrication, reduced parasitic effects, and seamless integration with rectifying circuits. Furthermore, CPW-fed antennas allow for flexible ground-plane modifications, which can be effectively exploited to enhance impedance bandwidth.

Various bandwidth enhancement techniques have been reported in the literature, including slot loading of radiating patches, defective ground structures (DGSs), and ground plane perturbations [1–5]. Slotting the radiating element alters the surface current distribution, introduces additional resonant modes [6], and increases the effective electrical length without enlarging the antenna's physical size [7]. Similarly, defective ground structures modify the current flow in the ground plane [8], leading to improved impedance matching and bandwidth enhancement. However, many reported designs either occupy large physical areas, exhibit limited bandwidth, or suffer from reduced radiation efficiency when implemented on low-cost substrates such as FR4.

In recent years, several CPW-fed slot and DGS-based antennas have been proposed for wideband applications [9]. Nevertheless, achieving simultaneous wide bandwidth, compact size, and stable radiation patterns remains a challenging task, particularly for RF energy harvesting systems that require consistent performance across a broad frequency range [10]. Additionally, many designs do not adequately address size reduction while maintaining high efficiency, which is essential for practical deployment [11–15].

In addition to conventional receiving antennas, recent research has increasingly explored metasurface-assisted RF energy-harvesting techniques to improve electromagnetic energy capture and wireless power transfer efficiency. Transparent rectifying metasurfaces have been investigated for simultaneous dual-band RF energy harvesting while preserving optical transparency [16]. Reconfigurable intelligent metasurfaces have also been proposed to dynamically enhance wireless power transfer and communication performance through adaptive electromagnetic wave manipulation [17]. Furthermore, spin-selective metasurfaces capable of achieving

* Corresponding author: Vijetha Rajappa (rvijetha9@gmail.com).

doi:10.2528/PIERC26051702

Published by THE ELECTROMAGNETIC ACADEMY

nearly perfect electromagnetic wavefront manipulation have demonstrated the significant potential of advanced metasurface technologies for future wireless systems [18]. Although these approaches provide attractive functionalities, they generally involve considerably higher structural complexity and fabrication requirements than conventional planar antennas. In contrast, the present work focuses on the development of a compact, low-cost, and experimentally validated wideband receiving antenna that can serve as the front-end element of future broadband RF energy-harvesting systems.

Although numerous CPW-fed slot antennas and defective ground structure (DGS)-based antennas have been reported for wideband wireless applications, simultaneously achieving compact size, wide impedance bandwidth, stable radiation characteristics, and simple low-cost implementation remains a significant challenge. Most reported designs employ slot loading, ground-plane modification, or feed optimization individually to improve impedance matching. However, relatively few studies have exploited the combined interaction among asymmetric CPW excitation, radiator perturbation, and defective ground engineering to realize multiple closely spaced resonant modes over a broad operating bandwidth while maintaining a compact footprint. Furthermore, the development of compact broadband receiving antennas suitable for future RF energy harvesting systems has received comparatively less attention than complete rectenna implementations, thereby motivating the present work.

The proposed antenna employs an embedded slotted rectangular radiator, asymmetric CPW excitation, dual-slot loading, and a hybrid hexagonal defective ground structure to simultaneously improve impedance matching, enhance electromagnetic coupling, and excite multiple closely spaced resonant modes while maintaining a compact footprint. The term "hybrid" refers to the combined bandwidth enhancement achieved through the interaction of these complementary design features rather than the ground slot geometry alone. This integrated design approach enables wideband operation while maintaining compact dimensions and stable radiation characteristics using a simple single-layer FR4 substrate.

The present work focuses on the design, optimization, fabrication, and experimental validation of the receiving antenna, which constitutes the first stage of a broadband RF energy harvesting (rectenna) system. The primary objective is to develop a compact wideband antenna capable of efficiently capturing ambient RF signals across multiple communication bands while maintaining stable radiation characteristics and high radiation efficiency. The integration of the proposed antenna with a broadband rectifier and the evaluation of RF-to-DC conversion efficiency are beyond the scope of the present study and will be investigated in future work.

In this work, a compact CPW-fed slotted rectangular patch antenna incorporating a hybrid hexagonal defective ground structure with linear polarization is proposed for wideband RF energy harvesting applications. The proposed antenna employs an embedded slotted radiator, asymmetric CPW excitation, and dual-slot loading to excite multiple closely spaced resonant modes while maintaining a compact footprint. As a result, the antenna achieves a measured impedance bandwidth from 2.18 GHz to 5.79 GHz (90.6% fractional bandwidth), covering 2.4/5 GHz WLAN bands and sub-6 GHz 5G spectrum. The antenna is fabricated on a low-cost FR4 substrate and experimentally validated via reflection coefficient, gain, radiation pattern, and radiation efficiency. Owing to its compact size, wide impedance bandwidth, stable radiation characteristics, and high radiation efficiency, the proposed antenna is well-suited as the receiving element of future broadband RF energy harvesting (rectenna) systems as well as wideband wireless communication applications.

2. ANTENNA GEOMETRY AND DESIGN PARAMETERS

The geometry of the proposed CPW-fed wideband antenna is shown in Fig. 1, with all critical dimensions annotated. The antenna is fabricated on an FR4 substrate of thickness $h = 1.6\,\text{mm}$, relative permittivity $\varepsilon_r = 4.4$, and loss tangent $\tan\delta = 0.02$, with an overall footprint of $40 \times 40\,\text{mm}^2$.

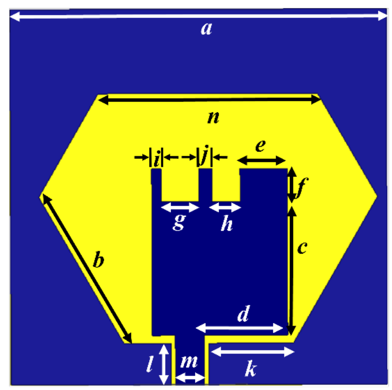

FIGURE 1. Proposed wideband antenna.

The radiating element is a rectangular patch of dimensions $17.75 \times 14.4\,\text{mm}^2$, positioned inside a hybrid hexagonal slotted ground plane to achieve compactness and wideband impedance matching. The hexagonal slot etched in the ground plane has an edge length of 18 mm, forming a defective ground structure (DGS) that modifies the surface current distribution and contributes to bandwidth enhancement. A coplanar waveguide (CPW) feed is employed, with a feed-line dimension of $5.25 \times 3.08\,\text{mm}^2$ and a CPW gap of 0.46 mm, ensuring a characteristic impedance of approximately $50\,\Omega$. The characteristic impedance of the CPW feed can be expressed as [19, 20]

$$Z_0 = \frac{30\pi}{\sqrt{\varepsilon_{\text{eff}}}} \frac{K(k')}{K(k)} \tag{1}$$

where K is the complete elliptic integral of the first kind,

$$k = \frac{W_f}{W_f + 2g} \tag{2}$$

$$k' = \sqrt{1 - k^2} \tag{3}$$

with W_f being the feed width and g the CPW gap. The feed dimensions are optimized to ensure proper impedance matching over the operating frequency band.

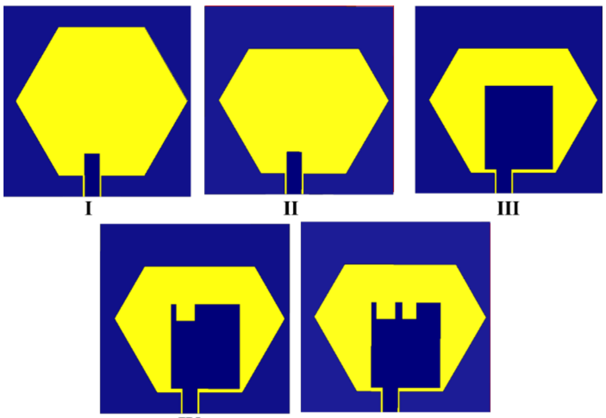

FIGURE 2. Design evolution of the proposed antenna.

To excite multiple resonant modes and improve impedance matching, the feed is intentionally placed off-center toward the left-hand side of the patch, rather than at the geometric center. This asymmetry perturbs the current distribution and assists in exciting higher-order resonant modes. Two rectangular slots are etched on the radiating patch to generate additional resonances. The first slot of size $3.5 \times 4\,\text{mm}^2$ is etched near the top-left corner of the patch, positioned 1 mm away from the patch edge, while the second slot of size $3.5 \times 3\,\text{mm}^2$ is etched at the center of the top edge. The separation between the two slots is maintained at 1.4 mm, ensuring controlled coupling between resonant modes.

The patch is vertically offset by 0.84 mm above the ground plane on the bottom side, which modifies the electromagnetic coupling between the patch and the ground plane and further alters the effective current path, assisting in wideband impedance matching. All optimized design parameters are summarized in Table 1.

TABLE 1. Optimized design parameters.

Parameter	a	b	c	d	e	f	g
Dimension (mm)	40	18	14.25	8.86	5	3.5	4
Parameter	h	i	j	k	l	m	n
Dimension (mm)	3	1	1.4	9	4.4	3.08	23

The initial dimensions of the radiating patch were estimated using the conventional microstrip antenna design methodology corresponding to the desired center frequency. Subsequently, the CPW feed dimensions were determined to realize a characteristic impedance of 50 Ω using (1)–(3). Owing to the introduction of an asymmetric CPW feed, a hybrid hexagonal defective ground structure, an embedded radiator configuration, and dual-slot loading, the analytical design equations provide only the initial design estimates. Therefore, all geometry parameters were further optimized using the full-wave electromagnetic simulator ANSYS High-Frequency Structure Simulator (HFSS) to obtain wide impedance bandwidth while maintaining compact dimensions and stable radiation characteristics.

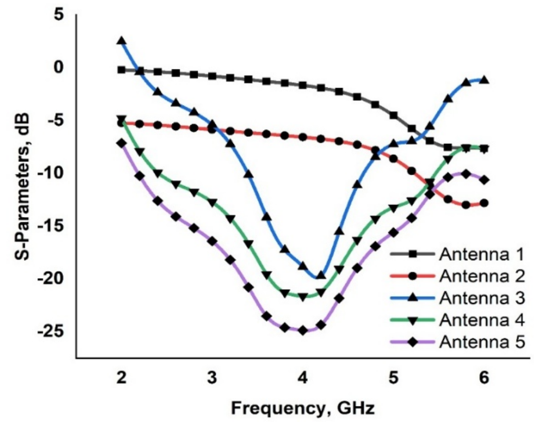

FIGURE 3. Simulated reflection coefficient during the antenna design evolution.

3. ANTENNA DESIGN EVOLUTION

The design evolution of the proposed antenna is illustrated in Fig. 2, and the corresponding simulated S_{11} responses are presented in Fig. 3. Initially, a rectangular strip line excited via CPW feeding and placed within a hexagonal slotted ground plane produced a single resonance around 5.8 GHz, though with poor impedance matching. Subsequently, the ground plane width was increased by 4.6 mm, which altered the electromagnetic coupling around the hexagonal slot, resulting in improved impedance matching at the resonant frequency. Replacing the strip line with a rectangular patch radiator extended the impedance bandwidth to approximately 3–5.5 GHz, indicating the excitation of multiple resonant modes.

To further enhance bandwidth, a $3.5 \times 4\,\text{mm}^2$ slot was etched near the top-left corner of the patch. This perturbation increased the effective electrical length of the surface current path, leading to improved matching at lower frequencies. Finally, an additional $3.5 \times 3\,\text{mm}^2$ slot etched at the center of the top edge of the patch introduced another resonant mode, resulting in a continuous wideband impedance response from 2.18 GHz to 5.79 GHz, corresponding to a total bandwidth of 3.61 GHz for $|S_{11}| \leq -10\,\text{dB}$.

The observed bandwidth enhancement is attributed to the progressive excitation and coupling of multiple resonant modes introduced by each design modification. The asymmetric CPW feed improves impedance matching by modifying the input current distribution, while the hybrid hexagonal defective ground structure alters the ground current path and enhances electromagnetic coupling between the radiator and the ground plane. The dual rectangular slots further perturb the surface current distribution, producing additional closely spaced resonant modes that merge to realize the measured wideband response.

4. PARAMETRIC ANALYSIS

To study the sensitivity of the proposed antenna to key geometrical parameters and to identify the dominant factors governing wideband operation, a parametric analysis was carried out using ANSYS HFSS. The effects of the first rectangular slot width, second rectangular slot width, and ground plane length

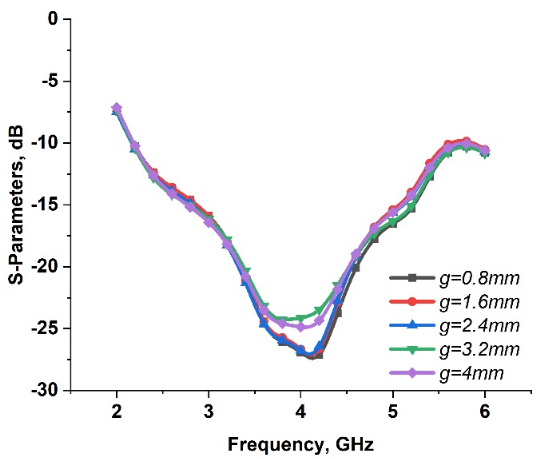

FIGURE 4. Simulated reflection coefficient for different values of the first rectangular slot width.

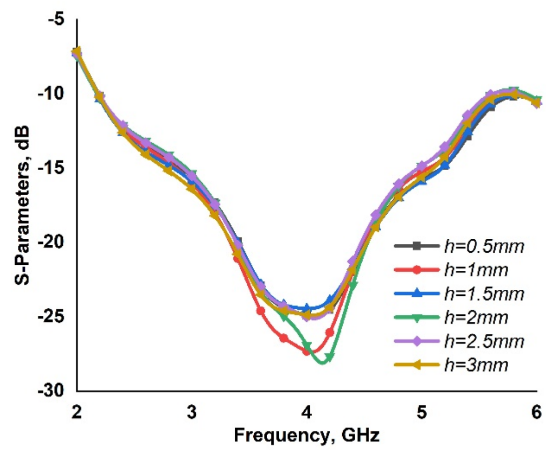

FIGURE 5. Simulated reflection coefficient for different values of the second rectangular slot width.

on the impedance characteristics are investigated while keeping all other parameters unchanged. The corresponding simulated reflection coefficients are shown in Figs. 4–6.

4.1. Effect of First Rectangular Slot Width

The effect of varying the width of the first rectangular slot, located near the top-left corner of the patch, on the reflection coefficient is shown in Fig. 4. The slot width is varied from 0.8 mm to 4 mm in steps of 0.8 mm.

Although variations in the width of the first rectangular slot produce only minor changes in the overall impedance bandwidth, the slot plays an important role in modifying the surface current distribution and improving impedance matching within the lower and middle portions of the operating band. The first slot perturbs the dominant current path, thereby enhancing electromagnetic coupling between the radiator and the hybrid hexagonal defective ground structure. Consequently, the first slot contributes primarily to impedance stabilization and mode tuning rather than bandwidth expansion.

4.2. Effect of Second Rectangular Slot Width

Figure 5 illustrates the effect of varying the width of the second rectangular slot, etched at the center of the patch's top edge. The slot width is varied from 0.5 mm to 3 mm in steps of 0.5 mm.

Similar to the first slot, the second rectangular slot has only a limited influence on the overall impedance bandwidth when its width is varied. However, its primary function is to facilitate coupling between adjacent resonant modes generated by the radiator and the defective ground structure. This controlled mode interaction results in a smoother impedance transition over the operating band, thereby improving impedance matching without significantly altering the overall bandwidth. Therefore, the second slot acts mainly as a mode-coupling element that contributes to the stable wideband response of the proposed antenna.

4.3. Effect of Ground Plane Length

The influence of ground plane length on impedance characteristics is shown in Fig. 6. The ground plane length is varied from 9 mm to 5 mm in steps of 1 mm.

In contrast to the slot parameters, the ground plane length exhibits a significant impact on both impedance bandwidth and resonant frequency location. A pronounced increase in bandwidth is observed as the ground plane length is reduced. Additionally, a clear shift of the operating frequency band toward lower frequencies is evident.

The parametric investigation demonstrates that the ground-plane length is a dominant parameter governing the operating bandwidth, while the two rectangular slots primarily optimize impedance matching and control the interaction among multiple resonant modes. Consequently, the proposed wideband performance is achieved through the combined action of the hybrid hexagonal defective ground structure, asymmetric CPW excitation, and slot loading rather than the influence of any individual parameter alone.

5. SIMULATED AND MEASURED RESULTS

The electromagnetic performance of the proposed wideband antenna is analysed using ANSYS HFSS and experimentally validated via measurements carried out using a Vector Network Analyzer (VNA) and an anechoic chamber. The simulated and measured results are presented and discussed in terms of reflection coefficient, gain, radiation efficiency, and radiation patterns, demonstrating good agreement and validating the effectiveness of the proposed design.

5.1. Reflection Coefficient (S_{11}) Analysis

The simulated and measured reflection coefficients of the proposed antenna are shown in Fig. 7. A good correlation between the simulated and measured results is observed across the entire operating band. The antenna exhibits a measured impedance bandwidth of 3.61 GHz, extending from 2.18 GHz to 5.79 GHz for the criterion $|S_{11}| \leq -10$ dB. This wideband response ef-

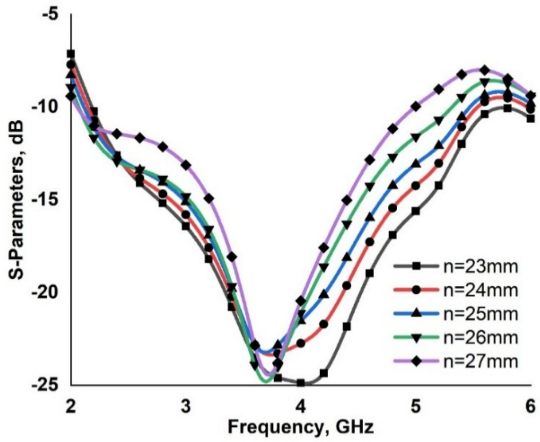

FIGURE 6. Simulated reflection coefficient for different ground-plane lengths.

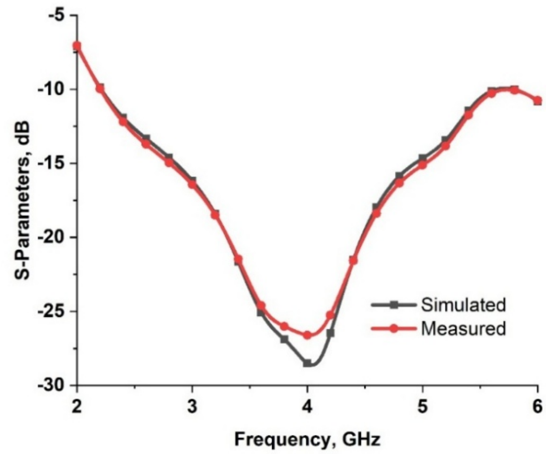

FIGURE 7. Simulated and measured S_{11}.

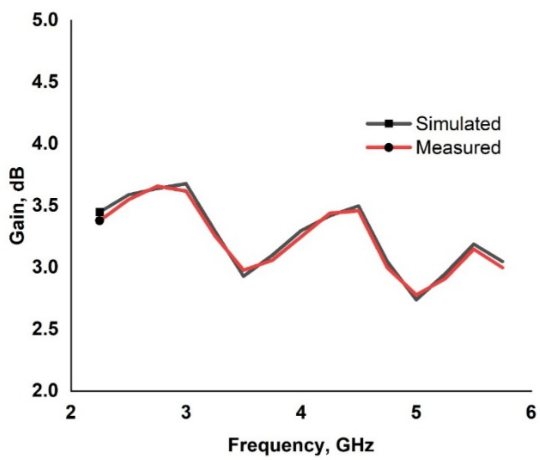

FIGURE 8. Simulated and measured gains.

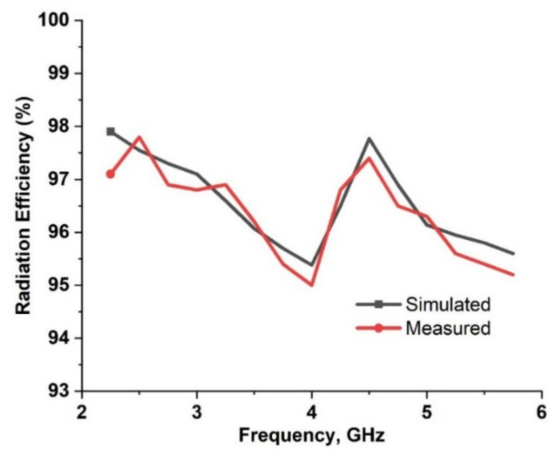

FIGURE 9. Simulated and measured radiation efficiencies.

fectively covers the 2.4 GHz Wi-Fi band as well as the sub-6 GHz 5G frequency range, making the antenna suitable for wideband wireless and RF energy harvesting applications.

Minor discrepancies between the simulated and measured results, particularly at higher frequencies, can be attributed to fabrication tolerances, SMA connector losses, soldering effects, and dielectric constant variations of the FR4 substrate. Nevertheless, the overall agreement confirms the reliability of the design methodology and optimization process.

5.2. Gain and Radiation Efficiency

The simulated and measured peak gain variations of the proposed antenna across the operating frequency band are illustrated in Fig. 8. The antenna achieves a maximum measured gain of 3.67 dB at 3 GHz, while the minimum gain of 2.73 dB is observed near 5 GHz. A relatively stable gain profile is maintained throughout the band, which is essential for wideband energy harvesting and communication systems.

Figure 9 presents the simulated and measured radiation efficiencies of the proposed antenna over the operating frequency band. A close agreement between the simulated and measured results is observed, confirming the reliability of the proposed design. The antenna exhibits radiation efficiency greater than 95% throughout the operating band, with a maximum value approaching 98%. Although FR4 possesses a relatively high dielectric loss tangent ($\tan\delta = 0.02$), the proposed antenna maintains high radiation efficiency owing to several design features. The CPW-fed configuration minimizes parasitic radiation and provides efficient impedance matching, while the hybrid hexagonal defective ground structure and optimized slot configuration improve electromagnetic coupling and reduce mismatch losses. Furthermore, the compact radiator geometry enables efficient excitation of the dominant resonant modes, resulting in effective radiation across the entire operating bandwidth. The close agreement between simulated and measured efficiencies further validates the effectiveness of the proposed antenna configuration.

5.3. Radiation Pattern Characteristics

The simulated and measured radiation patterns of the proposed antenna in the E-plane ($\varphi = 0°$) and H-plane ($\varphi = 90°$) at frequencies 2.5, 3, 3.5, 4, 4.5, and 5 GHz are shown in Fig. 10.

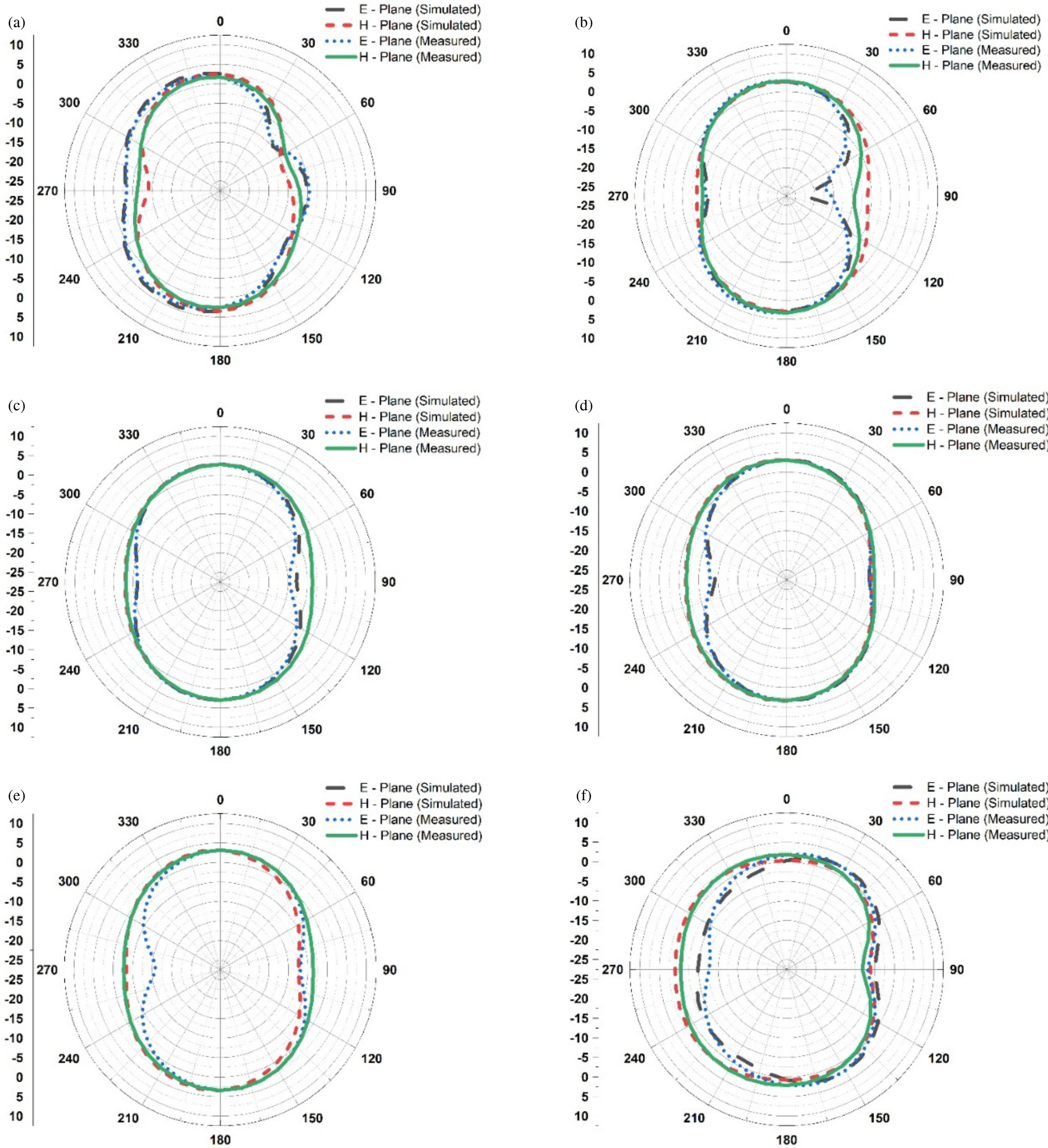

FIGURE 10. Simulated and measured radiation patterns (E-plane and H-plane) at different frequencies. (a) at 2.5 GHz, (b) at 3 GHz, (c) at 3.5 GHz, (d) at 4 GHz, (e) at 4.5 GHz, and (f) at 5 GHz.

Across the operating band, the antenna exhibits a stable figure-of-eight radiation pattern, which is a characteristic of CPW-fed planar antennas with defective ground structures. The patterns remain consistent with minimal distortion, indicating stable radiation behavior over the wide frequency range. Close agreement between simulated and measured radiation patterns is observed at all frequencies, validating the robustness of the proposed antenna design. Slight asymmetry in the measured patterns is attributed to measurement uncertainties, connector effects, and finite ground plane size.

Table 2 summarizes the measured half-power beamwidth (HPBW) of the proposed antenna in both the E- and H-planes at selected operating frequencies. The measured HPBW remains relatively stable throughout the operating band, demonstrating consistent radiation characteristics despite the excitation of multiple resonant modes. A slight variation in

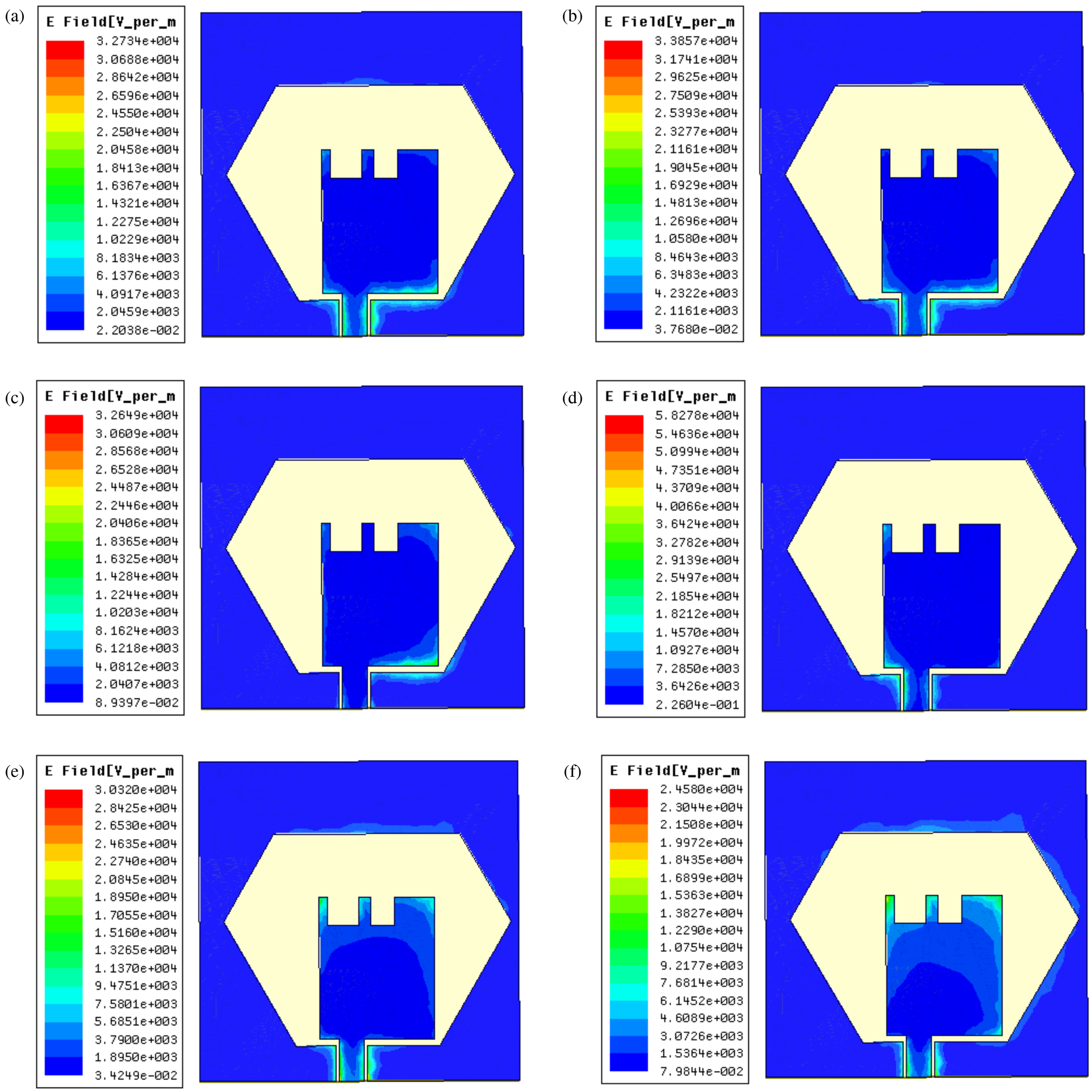

FIGURE 11. Simulated surface current distributions at different operating frequencies. (a) at 2.5 GHz, (b) at 3 GHz, (c) at 3.5 GHz, (d) at 4 GHz, (e) at 4.5 GHz, and (f) at 5 GHz.

beamwidth is observed with increasing frequency due to the redistribution of surface currents associated with higher-order resonant modes. At 5 GHz, the H-plane radiation pattern does not exhibit a distinct single main lobe; therefore, the HPBW is not reported for this case. Overall, the measured results confirm that the proposed antenna maintains stable radiation behavior over the entire operating bandwidth.

5.4. Surface Current Distribution and Electromagnetic Interpretation

To further understand the wideband operating mechanism of the proposed antenna, the simulated surface current distributions at 2.5, 3, 3.5, 4, 4.5, and 5 GHz are illustrated in Fig. 11. The current distributions reveal that different structural elements become dominant at different frequencies, thereby confirming the excitation of multiple closely spaced resonant modes responsible for the observed wide impedance bandwidth.

TABLE 2. Measured half-power beamwidth (HPBW) of the proposed antenna in the E-plane and H-plane at selected operating frequencies.

Frequency (GHz)	E-plane HPBW (°)	H-plane HPBW (°)
2.5	57.2	41.4
3.0	48.5	45.8
3.5	43.8	47.4
4.0	37.0	55.9
4.5	46.6	48.8
5.0	59.0	N/A

TABLE 3. Comparison with recently reported wideband antennas.

Ref. No	Substrate	Dimensions (λ)	Bandwidth	Peak Gain, dB	Efficiency (%)
1	FR4	$0.41\lambda_0 \times 0.33\lambda_0 \times 0.018\lambda_0$	3.3 GHz to 6 GHz	3.54	81
2	jeans	$0.63\lambda_0 \times 0.56\lambda_0 \times 0.014\lambda_0$	3.87 GHz to 5.914 GHz	2.98	87
3	FR4	$0.30\lambda_0 \times 0.30\lambda_0 \times 0.014\lambda_0$	2.56 GHz–4.3 GHz	5.7	90
4	FR4	$0.18\lambda_0 \times 0.28\lambda_0 \times 0.019\lambda_0$	3.6 to 5.5 GHz	6	90
This work	FR4	$0.29\lambda_0 \times 0.29\lambda_0 \times 0.012\lambda_0$	2.18 GHz to 5.79 GHz	3.67	97

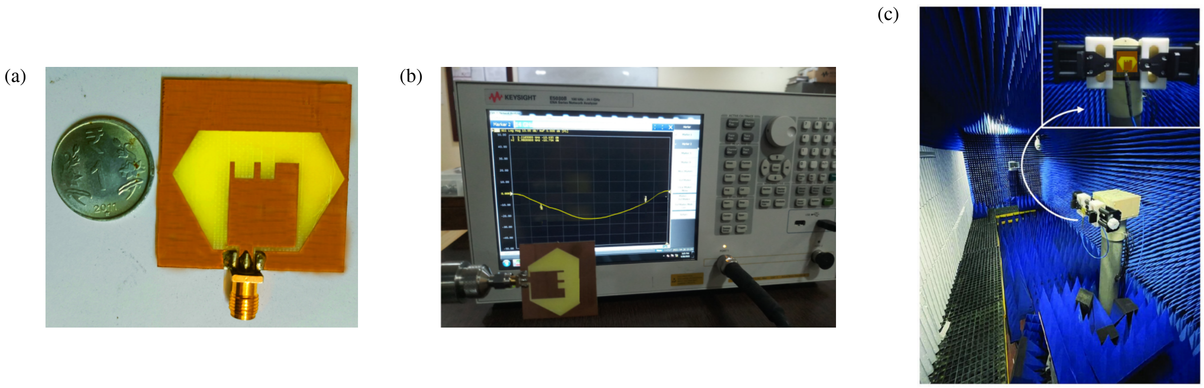

FIGURE 12. Fabricated antenna prototype and experimental measurement setup. (a) Fabricated antenna, (b) S_{11} measurement setup with VNA, and (c) antenna measurement setup in an anechoic chamber.

At 2.5 GHz, the surface current is predominantly concentrated along the outer edges of the rectangular radiator and around the lower portion of the hybrid hexagonal defective ground structure. The current follows a relatively long path, indicating excitation of the fundamental resonant mode responsible for the lower-frequency operation. At 3 GHz and 3.5 GHz, the current density increases around the asymmetric CPW-feed junction and the left rectangular slot. The slot perturbs the dominant current path and improves electromagnetic coupling between the radiator and the defective ground structure, thereby enhancing impedance matching across the lower and middle portions of the operating band.

At 4 GHz, strong current concentrations are simultaneously observed around both rectangular slots and edges of the hexagonal ground aperture. This indicates the coexistence of multiple resonant modes, whose mutual coupling results in a continuous impedance response rather than isolated narrowband resonances. At 4.5 GHz and 5 GHz, the current gradually shifts toward the upper portion of the radiator and the second rectangular slot, while significant current remains around teh edges of the defective ground structure. The shorter current paths excited at these frequencies correspond to higher-order resonant modes that extend the impedance bandwidth toward the upper end of the operating band. Overall, the observed current distributions confirm that the proposed wideband performance is not produced by a single resonant structure. Instead, the hybrid hexagonal defective ground structure, asymmetric CPW excitation, and dual-slot loading collectively generate multiple closely spaced resonant modes that merge to produce the measured continuous wideband response from 2.18 GHz to 5.79 GHz.

5.5. Measurement Setup

The fabricated antenna prototype together with the experimental measurement setup is shown in Fig. 12. The reflection coefficient (S_{11}) of the fabricated antenna was measured using a calibrated Vector Network Analyzer (VNA), while the radiation pattern, gain, and radiation efficiency were experimentally characterized in a standard anechoic chamber. The measured results exhibit good agreement with the corresponding full-wave electromagnetic simulations, thereby validating the proposed antenna design. Minor discrepancies between the simulated and measured characteristics are mainly attributed to fabrication tolerances, SMA connector effects, cable losses, measurement uncertainties, and slight variations in the dielectric properties of the FR4 substrate. All measurements were carried out under identical experimental conditions to ensure the consistency and repeatability of the measured results.

6. COMPARISON WITH EXISTING WORKS

To evaluate the performance of the proposed antenna, a comparison with recently reported wideband antennas is presented in Table 3. The key metrics considered include substrate type, antenna dimensions, impedance bandwidth, peak gain, and radiation efficiency, which are critical for wideband wireless and RF energy harvesting applications.

7. CONCLUSION

A compact CPW-fed wideband antenna with a hybrid hexagonal defective ground structure has been presented. The proposed design achieves a measured impedance bandwidth of 3.61 GHz, spanning 2.18–5.79 GHz, thereby covering the 2.4/5 GHz Wi-Fi and sub-6 GHz 5G frequency bands. The antenna exhibits a measured peak gain of 3.67 dB at 3 GHz and a minimum measured gain of 2.73 dB at 5 GHz, and a measured radiation efficiency greater than 95%, with a maximum value approaching 98% across the operating band. The wideband performance is achieved through a combination of off-center CPW feeding, patch slotting, and defective-ground engineering, as confirmed by parametric studies and surface-current analysis. Simulated and measured results demonstrate good agreement, validating the design methodology. The compact size, wide impedance bandwidth, and high radiation efficiency make the antenna suitable for RF energy harvesting and wideband wireless applications. Future work includes integrating the proposed antenna with a rectenna system for practical energy-harvesting implementations.

REFERENCES

[1] Omar, M. F. M., A. A. Manaf, M. F. Ain, and S. K. A. Rahim, "CPW-fed circular patch antenna with rectangular slot-loaded DGS for wideband application," *ELEKTRIKA-Journal of Electrical Engineering*, Vol. 24, No. 1, 7–13, 2025.

[2] Singh, G., A. P. Singh, Z. Ali, N. K. Sharma, and V. K. Singh, "An innovative DGS based textile antenna with semi-circular slot for future IoT's and AI applications," *Transactions on Electrical and Electronic Materials*, Vol. 26, No. 1, 78–103, 2025.

[3] Sekhar, M. and S. Nelaturi, "Wideband circular polarized meandered patch antenna for microwave imaging," *Analog Integrated Circuits and Signal Processing*, Vol. 111, No. 1, 81–88, 2022.

[4] Megahed, A. A., M. Abdelazim, E. H. Abdelhay, and H. Y. M. Soliman, "Sub-6 GHz highly isolated wideband MIMO antenna arrays," *IEEE Access*, Vol. 10, 19 875–19 889, 2022.

[5] Megahed, A. A., A. H. Hussein, A. J. A. Al-Gburi, and R. H. Elabd, "Compact wideband antenna array with DGS-based metamaterial for efficient smartphone communication and SAR reduction," *Progress In Electromagnetics Research B*, Vol. 110, 15–28, 2025.

[6] Tsegaye, A., X.-Q. Lin, H. Liu, and H. S. Abubakar, "A compact monopole wideband antenna based on DGS," *Electronics*, Vol. 14, No. 12, 2311, 2025.

[7] Prasad, R. K., A. Gupta, R. Dwivedi, N. Anand, U. Patel, and R. K. Verma, "Design and investigation of single wideband microstrip patch antenna with enhanced bandwidth for 5G/WiMAX/WLAN applications," *International Journal of Communication Systems*, Vol. 38, No. 14, e70240, 2025.

[8] Chen, H., H. Chen, W. Che, and Q. Xue, "A wideband V2X antenna with tilted beam pattern and transparent characteristics," *IEEE Antennas and Wireless Propagation Letters*, Vol. 24, No. 7, 1959–1963, Jul. 2025.

[9] Tan, S., L. Zhang, Q. Sun, B. Tang, and Q. Wang, "A design of a leaf-shaped biomimetic flexible wideband antenna," *Electronics*, Vol. 14, No. 13, 2620, 2025.

[10] Patel, K. and S. K. Behera, "Design of band reconfigurable Koch fractal antenna for wideband applications," *AEU — International Journal of Electronics and Communications*, Vol. 188, 155592, 2025.

[11] Sura, P. R. and M. Sekhar, "Circularly polarized dual band dual slot antenna for WLAN, Wi-MAX and Wi-Fi applications," *IETE Journal of Research*, Vol. 69, No. 3, 1550–1555, 2023.

[12] Rao, N. A., S. Kanapala, and M. Sekhar, "Wideband circular polarized binomial antenna array for L-band radar," in *Microelectronics, Electromagnetics and Telecommunications. Lecture Notes in Electrical Engineering*, Vol. 521, 279–287, Springer, Singapore, 2019.

[13] Sura, P. R., M. Sekhar, and K. A. Kumar, "Design of dual-band notched UWB antenna loaded with split ring resonators for wide band rejection," *International Journal of Electronics Letters*, Vol. 11, No. 1, 17–29, 2023.

[14] Sekhar, M. and S. Nelaturi, "Design of a sub-6 GHz wideband antenna with metasurface-based gain enhancement for 5G applications," in *2024 IEEE Microwaves, Antennas, and Propagation Conference (MAPCON)*, 1–5, Hyderabad, India, 2024.

[15] Sura, P. R., M. Sekhar, and K. K. Andhe, "Quad band printed antenna for Wi-Fi, WLAN, C-band and WiMAX applications," *Wireless Personal Communications*, Vol. 124, No. 1, 437–448, 2022.

[16] Dong, L., L. Si, B. Liu, Q. Shen, R. Niu, X. Bao, H. Sun, and W. Zhu, "An optically transparent rectifying metasurface for 2.4/5.8 GHz dual-band RF energy harvesting," *Applied Physics Letters*, Vol. 126, No. 1, 011705, 2025.

[17] Dong, L., L. Si, Y. Liu, Q. Shen, P. Tang, G. Wu, R. Niu, Q. Wu, and W. Zhu, "Speech-controlled reconfigurable intelligent metasurface for real-time wireless power transfer and communication," *Research*, Vol. 8, 0831, 2025.

[18] Si, L., Q. Shen, L. Dong, H. Zhang, C. Dang, X. Bao, and W. Zhu, "Crosstalk-free spin-selective metasurface for full-space wavefront manipulation with nearly 100% efficiency," *Advanced Optical Materials*, Vol. 14, No. 9, 2501041, 2026.

[19] Simons, R. N., *Coplanar Waveguide Circuits, Components, and Systems*, John Wiley & Sons, 2001.

[20] Gevorgian, S., L. J. P. Linner, and E. L. Kollberg, "CAD models for shielded multilayered CPW," *IEEE Transactions on Microwave Theory and Techniques*, Vol. 43, No. 4, 772–779, 1995.